The STIM1 CTID domain determines access of SARAF to SOAR to regulate Orai1 channel function

Archana Jha,[1] Malini Ahuja,[1] József Maléth,[1] Claudia M. Moreno,[1] Joseph P. Yuan,[2] Min Seuk Kim,[3] and Shmuel Muallem[1]

[1]Epithelial Signaling and Transport Section, Molecular Physiology and Therapeutics Branch, National Institute of Dental and Craniofacial Research, National Institutes of Health, Bethesda, MD 20892
[2]Department of Integrative Physiology, University of North Texas Health Sciences Center, Fort Worth, TX 76107
[3]Department of Oral Physiology, School of Dentistry, Wonkwang University, Iksan City, Jeonbuk 570-749, Republic of Korea

Ca^{2+} influx by store-operated Ca^{2+} channels (SOCs) mediates all Ca^{2+}-dependent cell functions, but excess Ca^{2+} influx is highly toxic. The molecular components of SOC are the pore-forming Orai1 channel and the endoplasmic reticulum Ca^{2+} sensor STIM1. Slow Ca^{2+}-dependent inactivation (SCDI) of Orai1 guards against cell damage, but its molecular mechanism is unknown. Here, we used homology modeling to identify a conserved STIM1(448–530) C-terminal inhibitory domain (CTID), whose deletion resulted in spontaneous clustering of STIM1 and full activation of Orai1 in the absence of store depletion. CTID regulated SCDI by determining access to and interaction of the STIM1 inhibitor SARAF with STIM1 Orai1 activation region (SOAR), the STIM1 domain that activates Orai1. CTID had two lobes, STIM1(448–490) and STIM1(490–530), with distinct roles in mediating access of SARAF to SOAR. The STIM1 (448–490) lobe restricted, whereas the STIM1(490–530) lobe directed, SARAF to SOAR. The two lobes cooperated to determine the features of SCDI. These findings highlight the central role of STIM1 in SCDI and provide a molecular mechanism for SCDI of Orai1.

Introduction

Store-operated Ca^{2+} channels (SOCs) are central components of the receptor-evoked Ca^{2+} signal that are activated in response to Ca^{2+} release from the ER (Parekh and Putney, 2005). Ca^{2+} influx through SOCs mediates the plethora of Ca^{2+}-dependent cell functions (Parekh and Putney, 2005; Lee et al., 2010). The two components of the channels are the ER Ca^{2+} sensor STIM1 (Liou et al., 2005; Roos et al., 2005) and the pore-forming Orai1 (Feske et al., 2006; Vig et al., 2006; Zhang et al., 2006). Previous work defined several STIM1 domains that mediate Orai1 activation and regulation. The ER resident STIM1 N terminus has an EF hand and SAM domain, with Ca^{2+} released from the EF hand leading to oligomerization and clustering of STIM1 into puncta at the ER–plasma membrane junctions to activate Orai1 (Stathopulos et al., 2008, 2009). The cytoplasmic C terminus of STIM1 consists of coiled-coil domain 1 (CC1), STIM1 Orai1 activation region (SOAR), serine/proline-rich domain, and polybasic lysine-rich region. The SOAR domain (344–442; also known as CAD [Park

et al., 2009] and Ccb9 [Kawasaki et al., 2009]) binds to and fully activates the Orai channels (Kawasaki et al., 2009; Park et al., 2009; Yuan et al., 2009).

CC1 was suggested to interact with SOAR and keep it in an inactive state (Korzeniowski et al., 2010; Muik et al., 2011). In one model the interaction was proposed to be caused by coiled-coil interactions that are stabilized by hydrophobic interactions (Muik et al., 2011) and the second model proposed electrostatic interaction among four conserved glutamates (317–321) in CC1 and four conserved lysines (384–389) in SOAR (Korzeniowski et al., 2010). In the context of full-length STIM1, mutation of the acidic glutamates resulted in constitutively active STIM1 that clusters in the absence of store depletion, and mutations of the basic lysines in SOAR resulted in inactive STIM1 (Korzeniowski et al., 2010). More direct information became available recently with determination of the crystal structure of the SOAR domain and a short helix of CC1 that includes the conserved glutamates (Yang et al., 2012). The structure revealed that SOAR exists as a V-shaped dimer

The Rockefeller University Press $30.00
J. Cell Biol. Vol. 202 No. 1 71–79
www.jcb.org/cgi/doi/10.1083/jcb.201301148

JCB 71

(Yang et al., 2012), as was found earlier biochemically (Yuan et al., 2009). In the structure, the basic residues in SOAR are located close to the tip in the V structure and the acidic residues in the CC1 are distant from the basic residues in SOAR.

The function and regulation of the Orai1 channel have been extensively characterized. Orai1 functions as a highly Ca^{2+}-selective, inward-rectifying channel (Derler et al., 2012; Engh et al., 2012). Orai1 is prominently regulated by its ligand Ca^{2+} that inactivates the channel. The two known modes of inactivation are fast Ca^{2+}-dependent inactivation (FCDI) with $\tau_{1/2}$ of ∼10 and 100 ms (Hoth and Penner, 1993; Derler et al., 2009; Mullins et al., 2009) and slow Ca^{2+}-dependent inactivation (SCDI) that takes 2–3 min (Zweifach and Lewis, 1995; Parekh, 1998). A conserved negatively charged cluster in STIM1(475–483) is required for FCDI (Derler et al., 2009; Lee et al., 2009; Mullins et al., 2009) in conjunction with calmodulin binding domain of Orai1 (Mullins et al., 2009). The factors/mechanisms mediating SCDI and the role of STIM1 in SCDI are still obscure. However, a new protein named SARAF was reported recently to interact with STIM1 and facilitate SCDI (Palty et al., 2012). Human SARAF is a 339–amino acid long protein with a predicted single transmembrane domain and has an N terminus facing the ER lumen and a cytoplasmic C terminus. How SARAF interacts with STIM1 and mediates SCDI is not known.

In the present study, homology modeling of the conserved cytoplasmic STIM1(234–535) ERM domain was performed based on the crystal structure of SOAR (Yang et al., 2012). The SOAR portion of the model exhibits a high degree of homology with the crystal structure of SOAR and correctly predicts the position of the CC1 inhibitory helix with the four glutamates and the position of the four lysines in SOAR. The model predicts a highly conserved STIM1(447–530) domain C terminal to SOAR at the boundary of SOAR dimerization. We named this domain the C-terminal inhibitory domain (CTID) because perturbing this region resulted in constitutive, store-independent clustering of STIM1 and activation of Orai1. Molecular, biochemical, and functional studies reveal that CTID functions to determine access of SARAF to SOAR to regulate both FCDI and SCDI. In the resting state SARAF binds to SOAR in STIM1 and activation of Orai1 requires dissociation of SARAF to release SOAR and allow it to interact with and activate Orai1. Interestingly, all forms of activation of STIM1, including mutation in CC1, the EF hand mutant D76A, and deletion of CTID prevent access of SARAF to SOAR. These findings provide a molecular mechanism to explain SCDI and the regulation of STIM1 by SARAF to activate Orai1 and Ca^{2+} influx.

Results

Identification of CTID
Previous work showed that the SOAR domain is sufficient to fully activate the Orai channels (Yuan et al., 2009) and that SOAR is sequestered within STIM1 in part by CC1 (Korzeniowski et al., 2010; Muik et al., 2011). How SOAR is sequestered and how the sequestration is regulated during activation of Ca^{2+} influx is not known. The structures of the human and *Caenorhabditis*

elegans SOAR reported recently (Yang et al., 2012) offered an opportunity to begin to address these questions. Because the cytoplasmic domain of STIM1(234–685) activates Orai1 and retains key regulatory functions of STIM1 (Huang et al., 2006; Korzeniowski et al., 2010), it was submitted to the structure prediction sites Robetta and I-Tasser for homology modeling, which generated nine different structures. Most structures have poor (I-Tasser) to intermediate Q-mean scores, but upon further analysis of STIM1(234–530) one of the structures shown in Fig. S1 d closely predicted the structure of SOAR and the relative position of the short CC1 helix αA, the position of the four glutamates in CC1 and the four lysines in SOAR (Fig. S1, b and d), and SOAR alignment with the reported crystal structure (Fig. S1 c). Alignment of the CC1 helix αA could not be performed because the sequences of the human and *C. elegans* helices are not conserved. The STIM1 ERM domain that includes CC1, SOAR, and STIM1(447–535) is highly conserved and thus we focused on this domain. The model predicts that the domain C terminal to SOAR is in position to interfere with dimerization of SOAR that is required for activation of Orai1 (Yang et al., 2012). We reasoned that this domain might regulate activation of SOAR and thus named it the CTID. CTID is highly conserved among all the vertebrates (Fig. S2) and to study its function we generated several deletions based on the predicted helices, as depicted in Fig. S1 (a and d).

CTID Functions as an inhibitory domain
To analyze the function of CTID, we deleted the entire CTID and fragments within from STIM1 and determined the effect of the deletions on $[Ca^{2+}]_i$ (native SOC) and on Orai1 current. Fig. 1 a shows that deletion of CTID (STIM1(448–530)) and the smaller fragments STIM1(447–460) (Δ447–460), STIM1(448–490) (Δ448–490), STIM1(490–521) (Δ490–521), and STIM1(448–521) (Δ448-521) markedly activated Ca^{2+} influx in the absence of store depletion, as expected from deletion of an inhibitory domain. Accordingly, all STIM1 deletion constructs spontaneously clustered when expressed alone or with Orai1. Selective examples of clustering in the absence of Orai1 are shown in Fig. S3. Activation of Ca^{2+} influx and clustering required intact SOAR domain. Fig. 1 b shows that mutation of the four lysines in SOAR eliminated activation of Ca^{2+} influx by the deletion of CTID and of Δ447-460. Fig. 1 (c and d) shows that the deletion constructs also activated Orai1 current in the absence of store depletion, similar to SOAR. The extent of constitutive activity as compared with the peak current value was as follows: SOAR, 89 ± 5%; Δ448–521, 84 ± 3%; Δ447–460, 73 ± 11%; and Δ490–521, 73 ± 7%. The small differences in the maximal spontaneous currents likely reflect partial interaction of the constructs showing smaller spontaneous current with SARAF (see Fig. 3). Hence, CTID functions to maintain STIM1 in an inactive state and disruption of this domain by any of the deletions tested resulted in release of SOAR and activation of Ca^{2+} influx and Orai1.

CTID regulates FCDI and SCDI
CTID includes the negatively charged sequence [475]DDVDD-MDEE[483] reported to participate in FCDI of Orai1 (Derler et al., 2009; Lee et al., 2009; Mullins et al., 2009). Therefore,
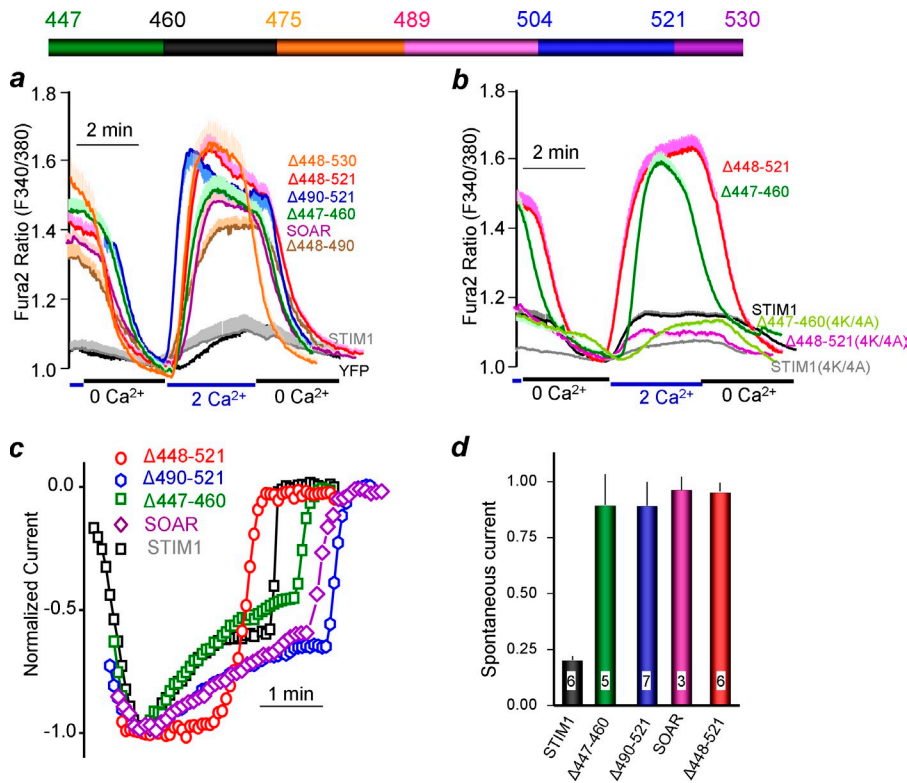
Figure 1. **Store-independent, spontaneous activity of STIM1 deletion mutants.** (a and b) Ca^{2+} influx was measured in HEK cells loaded with Fura2 and alternately perfused with Ca^{2+}-free and Ca^{2+}-containing solutions. The traces are mean ± SEM recorded from 30–40 HEK293 cells from three experiments transfected with YFP or the indicated STIM1 deletion mutants (a) and mutants in which four lysine residues in SOAR (384–387) were mutated to alanine (b). (c) Example traces of normalized whole cell current at −100 mV measured in HEK cells expressing mCherry-Orai1 and the indicated YFP-STIM1 C-terminal deletion mutants. Pipette solution contained 10 mM BAPTA and external solution contained 10 mM Ca^{2+}. Current measurement started within 10 s of break-in to evaluate the spontaneous current. The summary of multiple experiments is given in panel d, which shows the mean ± SEM of mean spontaneous current of the indicated number of cells.

we determined the effect of deleting CTID and CTID fragments on Orai1 inactivation. FCDI was measured after Orai1 activation by store depletion with 10 mM EGTA. As reported before, Fig. 2 (a and b) shows that Orai1 activated by SOAR does not undergo FCDI observed with wild-type STIM1 (Derler et al., 2009; Lee et al., 2009; Mullins et al., 2009). FCDI is also eliminated by deletion of CTID and of Δ448–521 but not of Δ490–521. However, unexpectedly, FCDI was also nearly eliminated by Δ447–460 and Δ490–504, although they include the

negatively charged sequence. FCDI with STIM1 was fitted by two exponentials with $\tau_1 = 12.3 \pm 1.2$ and $\tau_2 = 69.3 \pm 6.4$ ms, whereas Δ447–460 ($\tau_1 = 25 \pm 7$) and Δ490–504 ($\tau_1 = 22 \pm 4$) showed small and slower τ_1 and lost τ_2 (Fig. 2, example fits and fitness are shown in the inset; and results are summarized in Table S1). Deletion of STIM1(460–475) and of STIM1(475–490) resulted in a STIM1 mutant that strongly inhibited SOC and Orai1 (as discussed later). The findings with Δ447–460 and Δ490–504 indicate that the negatively charged sequence is
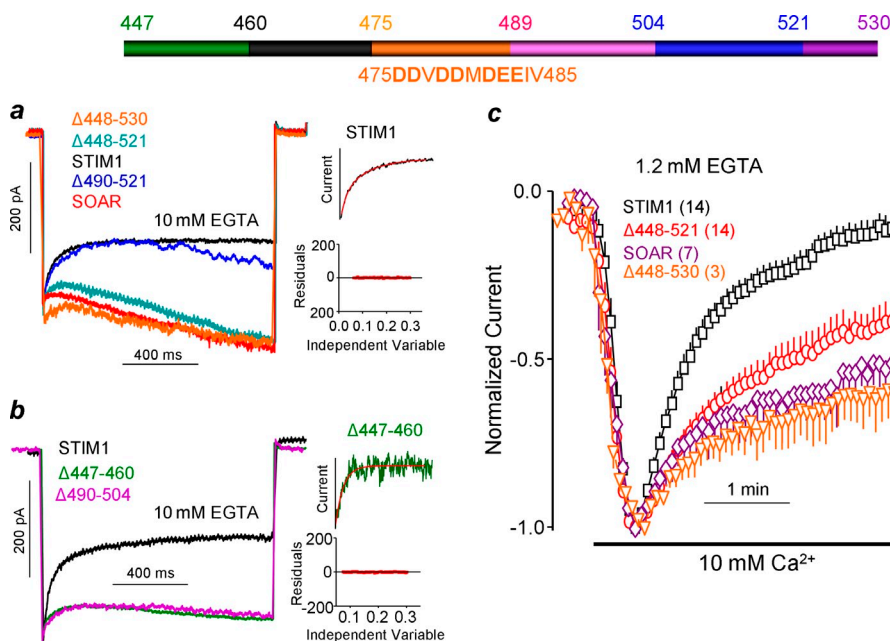

Figure 2. **FCDI and SCDI of Orai1 current activated by STIM1, SOAR, and STIM1 C-terminal deletion mutants.** (a and b) Example traces of FCDI of Orai1 current activated by the indicated STIM1 mutants was measured in pipette solution containing 10 mM EGTA and external solution containing 10 mM Ca^{2+}. For fast inactivation, −100 mV step voltage pulse of 1-s duration were applied when the current was fully developed. Table S1 shows the mean of 5–10 experiments similar to those in a and b of time constants (τ_1 and τ_2) obtained by fitting the current traces with double or single exponential functions, whichever was appropriate, and extent of inactivation. Example of double (STIM1) and single (STIM1Δ447–460) exponential fits and the quality of the fits (residuals) are shown in the insets. (c) Normalized averaged whole cell current levels at −100 mV measured in HEK cells expressing Orai1 and the indicated STIM1 C-terminal deletion mutants. Pipette solution contained 1.2 mM EGTA and 10 mM Ca^{2+} was added to the bath at the time indicated, 5 min after establishing the whole cell configuration. Table S1 shows the extent of inactivation in each case. The results are given as mean ± SEM of the number of experiments listed in parentheses.

Figure 3. **Coimmunoprecipitation of SARAF with SOAR and STIM1 mutants.** The STIM1 proteins are tagged with YFP and SARAF with Myc. Anti-YFP and anti-Myc were used for detection of protein expression and coimmunoprecipitation. All proteins were expressed in HEK cells. (a) SARAF interacts with SOAR but not with disrupted SOAR(4K/4A). (b) STIM1 CC1 (233–342) and STIM1(445–550) that includes CTID do not interact with SARAF, whereas SOAR (STIM1(344–442)), STIM1 (233–460), and STIM1(233–535) that include SOAR interact with SARAF. Controls were performed with each construct in the absence of precipitating antibodies. (c) The STIM1Δ447–460 and STIM1Δ475–490 mutations increased interaction whereas the STIM1Δ448–521 and STIM1Δ448–530 mutations markedly reduced binding of STIM1 with SARAF. (d) Coimmunoprecipitation of STIM1, Δ447–460, Δ475–490, and their 4K/4A mutants in SOAR, SOAR, and STIM1(344–485) with SARAF. The 4K/4A mutation markedly reduced the interaction with SARAF. One lane, which tested the effect of the 4E mutation on Δ475–490, marked by the gap was deleted for presentation purposes. The effect of this mutation is shown and is discussed in relation to Fig. 6 c. (e) Summary of the coimmunoprecipitation of the indicated deletions and number of experiments. The binding was normalized to input and used to calculate fold change relative to STIM1. Asterisk denotes P < 0.01 or better relative to STIM1.
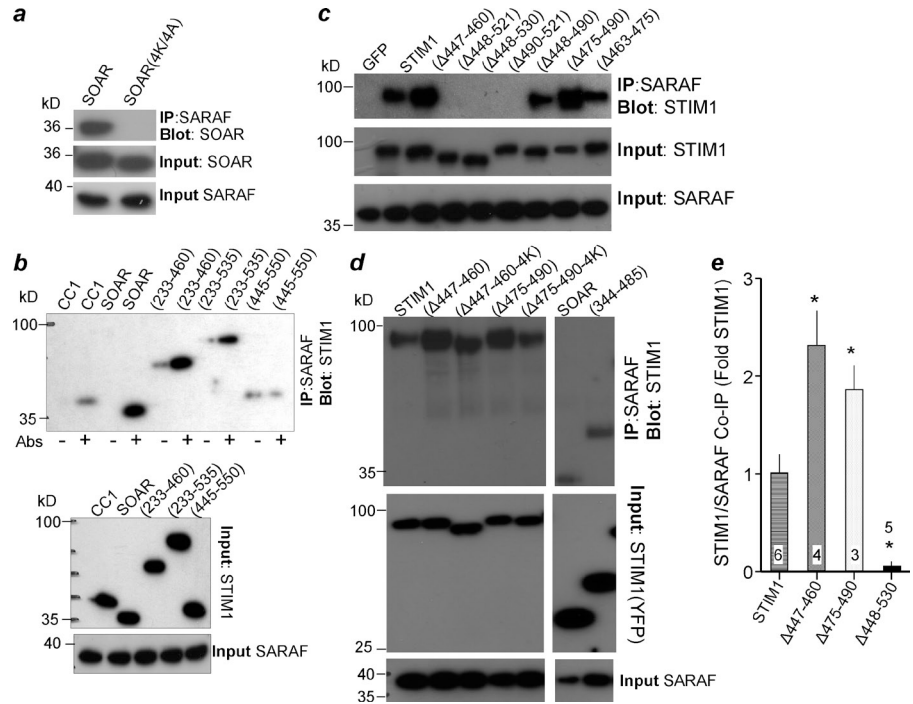
not sufficient for FCDI and requires additional elements of CTID, in particular the flanking STIM1(490–504) and STIM1 (448–475) or at least STIM1(447–460).

A key regulatory mode of Orai1 is the SCDI that inactivates Orai1 over several minutes to restrict Ca^{2+} influx and prevent cell toxicity (Parekh and Putney, 2005). The role of STIM1 in SCDI and the mechanism and regulation of SCDI is not known. To determine a role of CTID in SCDI, we measured Orai1 current in the presence of a low concentration of EGTA (1.2 mM) to facilitate the measurement of SCDI (Zweifach and Lewis, 1995). The results are shown in Fig. 2 c. After store depletion by dialysis with 1.2 mM EGTA for 5 min in the absence of external Ca^{2+}, the CRAC current was initiated by addition of 10 mM Ca^{2+} to the bath. Under these conditions the current evoked by STIM1 and Orai1 inactivated by 76 ± 4% within 2.5 min of current initiation. Orai1 activated by SOAR showed only 39 ± 7% inactivation. Deletion of CTID and Δ448–521 reduced SCDI to 32 ± 9% and 44 ± 6%, respectively, similar to the findings with SOAR.

CTID controls interaction of SARAF with SOAR

Recently, it has been reported that a single membrane span, ER-localized protein named SARAF facilitates SCDI of Orai1 current (Palty et al., 2012). The SARAF binding domain in STIM1 and the possible effect of CTID on SARAF function is not known. To address these issues, we first measured interaction of SARAF with SOAR and the STIM1 deletion mutants. Fig. 3 a shows that SARAF coimmunoprecipitates with SOAR and, importantly, mutation of the four lysines in SOAR

(SOAR(4K/4A)) eliminates the interaction. In Fig. 3 (b and d), we assayed the coimmunoprecipitate of SARAF with several constructs within the STIM1 ERM domain (233–535) and show that all constructs that include SOAR interact with SARAF, but the CTID-inclusive STIM1(445–550) does not. Hence, it is clear that SARAF interacts with a wild-type, functional SOAR.

Next we tested how deletion of CTID and fragments within CTID affect interaction of SARAF with STIM1. Fig. 3 c shows that deletion of CTID, STIM1(448–521), and the C terminal lobe of CTID, STIM1(490–521), nearly eliminated interaction of STIM1 with SARAF. In contrast, deletion of the N-terminal lobe of CTID, STIM1(448–489), or STIM1(463–475) had no effect on the interaction of STIM1 with SARAF, whereas Δ447–460 and Δ475–490 showed prominent enhanced interaction with SARAF (Fig. 3 e). Fig. 3 d shows that the enhanced interaction of Δ447–460 and Δ475–490 was markedly reduced by disruption of SOAR with the 4K/4A mutation.

Further evidence for enhanced interaction of Δ447–460 and Δ475–490 with SARAF and elimination of the interaction by STIM1(ΔCTID) was obtained by determining their localization. Fig. 4 shows that Δ448–490, Δ447–460, and Δ475–490 localize at a near plasma membrane domain and recruit SARAF to this domain. In contrast, STIM1(ΔCTID) that also localized at a near plasma membrane domain had no effect on SARAF localization, which remained in the ER.

The findings in Figs. 3 and 4 suggest that CTID controls access of SARAF to SOAR. To study the functional significance of this, we analyzed the role of CTID in SARAF-mediated facilitation of SCDI. The results are shown in Fig. 5 and the extent
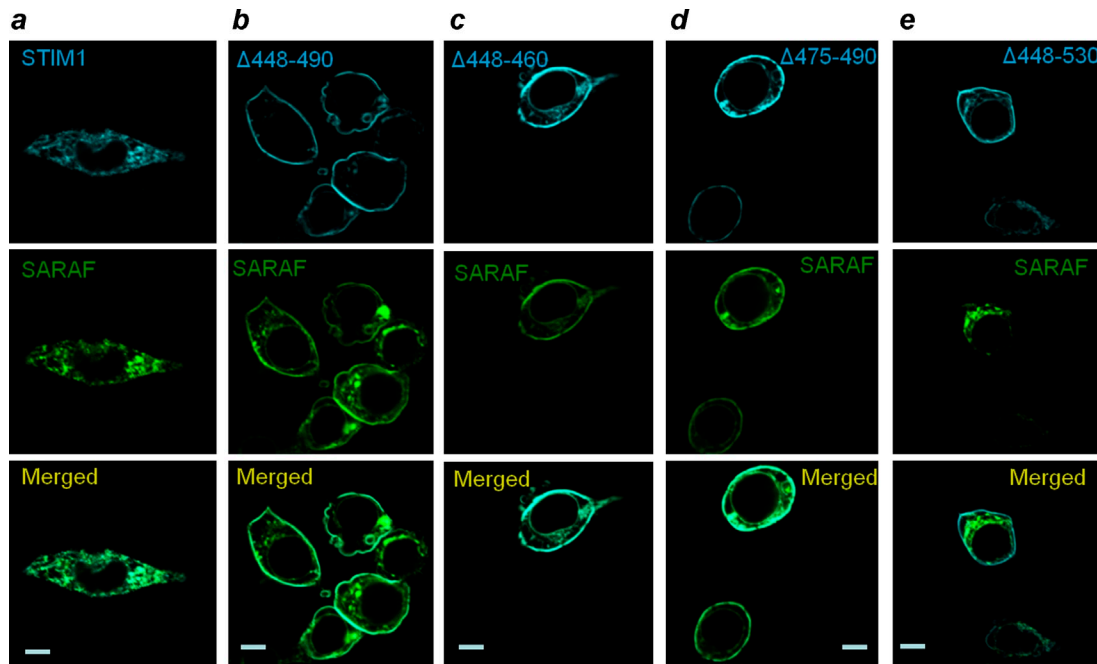
Figure 4. **The STIM1 mutants with enhanced binding recruit SARAF to the plasma membrane.** CFP-tagged STIM1 and deletion constructs and GFP-tagged SARAF were expressed in HEK cells and imaged after 16–24 h. The images show that STIM1Δ447–460 and STIM1Δ475–490 localize in the plasma membrane and recruit SARAF. STIM1Δ448–530 also localizes to the plasma membrane but does not affect SARAF localization. Bars, 5 µm.

of inhibition is listed in Table S1. $[Ca^{2+}]_i$ measurement shows that the store-independent activation of Ca^{2+} influx by SOAR and Δ447–460 was inhibited by SARAF. However, activation of Ca^{2+} influx by ΔCTID (Δ448–530), Δ448–521, and Δ490–521 was not affected by SARAF. Fig. 5 b shows that the SCDI measured with STIM1 is strongly reduced by siSARAF to the SCDI measured with SOAR and with ΔCTID. Fig. 5 (c and d) shows that SARAF increased the extent of SCDI of the Orai1 current activated by STIM1 and SOAR, while not affecting the current activated by ΔCTID. The CTID site that controls SARAF function was further narrowed by the finding that Δ490–521 reduced SCDI and eliminated the effect of SARAF (Fig. 5 d), whereas SCDI by Δ448–490 was highly increased by SARAF (Fig. 5 e). This suggests that STIM1(490–521) controls the effect of SARAF. This conclusion is further supported by the behavior of deletion of STIM1(448–490). Δ447–460 increased the rate and extent of SCDI (Fig. 5, b and e), which was markedly reduced by siSARAF (Fig. 5 b) to the level measured with ΔCTID, and SARAF further inhibited the current measured with Δ447–460 (Fig. 5 e). Δ475–490 clustered at the plasma membrane but, nevertheless, strongly inhibited the native SOC activity (Fig. S4). Clustering and inhibition of Ca^{2+} influx required functional SOAR because the clustering was inhibited by the 4K/4A mutation in SOAR. The inhibition of Ca^{2+} influx by Δ475–490 was lost by the 4E/4A mutation in CC1 of Δ475–490 (Fig. S4), likely as a result of reduced interaction of Δ475–490(4E/4A) with SARAF. Inhibition of SOC was also eliminated by knockdown of SARAF, suggesting that deletion of STIM1(475–490) enhances SARAF interaction with STIM1. The Δ460–475 mutant is not active and partially inhibits SOC (unpublished data).

When SOAR is active SARAF does not bind to STIM1

The self-clustering and constitutive activation of Ca^{2+} influx by STIM1 with deleted CTID raised the question of whether other STIM1 mutants that activate Ca^{2+} influx in the absence of store depletion also affect interaction of STIM1 with SARAF and thus SCDI. We tested this possibility using two STIM1 mutants: STIM1 in which the four negatively charged glutamates in CC1 were mutated to alanines (Korzeniowski et al., 2010) and the D76A mutation in the EF hand (Liou et al., 2005). Fig. 6 a shows that STIM1(D76A) and STIM1(4E/4A) potently activate Ca^{2+} influx in the absence of store depletion and this influx is not inhibited by SARAF. Fig. 6 b shows the slow rate and extent of SCDI of the Orai1 current activated by STIM1(4E/4A) and STIM1(D76A) (33 ± 7%), which was unaffected by SARAF. Moreover, 4E/4A mutations in Δ447–460 eliminated the strong inhibition of the current by SARAF (compare Figs. 5 e and 6 b). Fig. 6 (c and d) shows that the D76A mutant and mutating the four glutamates in STIM1 and in the indicated STIM1 deletion constructs markedly reduce their interaction with SARAF. Equally important, disruption of SOAR by mutating the four lysines reduced interaction with SARAF in all STIM1 deletion mutants as well. Hence, in fully activated STIM1, SARAF does not access SOAR and, consequently, Orai1 current by activated STIM1 does not undergo SCDI.

We noticed that even with the fully active STIM1(ΔCTID), STIM1(4E/4A), and STIM1(D76A), some inactivation (∼30%) was still evident and SARAF had no effect on this inactivation. To test if this inactivation is mediated by Ca^{2+} we measured the inactivation in the presence of 10 mM BAPTA (fast Ca^{2+} buffer). Fig. S5 shows that in the presence of BAPTA the slow

Figure 5. CTID controls SCDI by SARAF. (a) Effect of SARAF on store-independent Ca²⁺ influx was measured in HEK293 cells transfected with STIM1, SOAR, and the indicated deletion mutants and SARAF. The traces are the means of 30–40 cells and shown as mean ± SEM. SARAF inhibited Ca²⁺ influx by SOAR, STIM1(Δ447–460), and STIM1(Δ448–490) but not by STIM1(Δ490–521), STIM1(Δ448–521), and STIM1(Δ448–530). (b) siSARAF reduces SCDI. HEK cells were treated with siSARAF for 48 h that reduced SARAF mRNA by 70% (right). The cells were then transfected with Orai1 and either STIM1 or STIM1(Δ447–460). The Orai1 current was measured 24 h after transfection. The results are plotted as normalized mean ± SEM current at −100mV of the number of experiments indicated in parentheses. Note that STIM1(Δ447–460) increased the rate of SCDI whereas siSARAF markedly reduced SCDI. (c–e) The mean ± SEM of the normalized current at −100 mV measured in HEK cells transfected with Orai1 and the indicated STIM1 C-terminal deletion mutants in the presence and absence of SARAF. Current measurement started by perfusing a solution containing 10 mM Ca²⁺ after 5-min incubation in Ca²⁺-free solution in whole cell configuration with pipette solution containing 1.2 mM EGTA. Note that SCDI is markedly reduced when Orai1 is activated by SOAR, STIM1(Δ490–521), and STIM1(Δ448–530) (c and d), whereas SCDI is accelerated with STIM1(Δ447–460) and STIM1(Δ448–490) (e). In addition, SARAF increased SCDI recorded with STIM1 and SOAR (c), had no effect with STIM1(Δ490–521) and STIM1(Δ448–530) (d), and potently inhibited Orai1 current activated by STIM1(Δ447–460) and STIM1(Δ447–460) (e). In panel e, after normalization, the currents were adjusted to the maximal currents to illustrate the inhibition of the current by SARAF. The dashed traces in d and e mark the SCDI recorded with STIM1 (control).
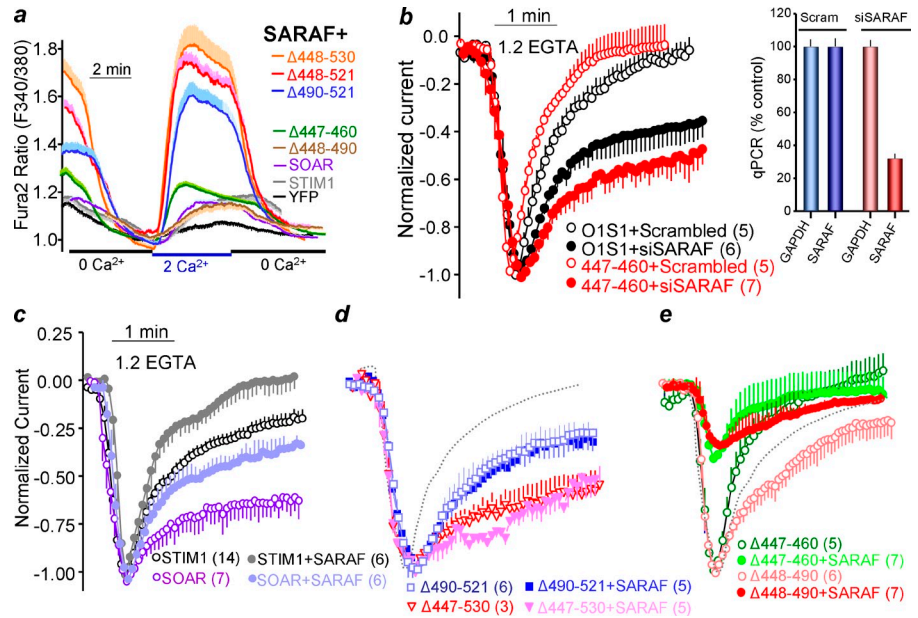
inactivation was nearly eliminated when Orai1 was activated by STIM1, SOAR STIM1(ΔCTID), STIM1(4E/4A), or STIM1(D76A) and that SARAF had no further effect. This suggests that the residual inactivation is also SCDI and thus SCDI has two components, one that is mediated by SARAF and one that is independent of SARAF. The nature and regulation of the SARAF-independent SCDI is unknown at present.

Discussion

The present study provides molecular information on the mechanism of SCDI of the Orai1 current, a key regulatory mode of Ca²⁺ influx. We discovered that the STIM1(448–530) domain C terminal to SOAR functions as an inhibitory domain that regulates the access of the STIM1 inhibitor SARAF to the STIM1 activation domain SOAR. We named this domain CTID to reflect its location and function. CTID is highly conserved in all vertebrates (Fig. S2). The combined findings of the interaction of SARAF with the STIM1 constructs (Figs. 3, 4, 6, S3, and S4) and the effects of SARAF on [Ca²⁺]ᵢ and the Orai1 current (Figs. 5, 6, and S4) led to several conclusions: (a) because deletion of CTID eliminates SCDI, CTID is the STIM1 domain that controls SCDI of Orai1; (b) SARAF coimmunoprecipitates with SOAR, but not with STIM1 or constitutively active STIM1 constructs with disrupted SOAR, indicating that SARAF interacts with SOAR to mediate the SCDI; (c) because deletion of CTID eliminates interaction of SARAF with STIM1 and STIM1(490–530) within CTID is required for interaction of SARAF with SOAR, CTID determines access of SARAF to SOAR to facilitate the SCDI; and (d) the STIM1(448–490) and STIM1(490–530) lobes cooperate to control access of SARAF to SOAR.

CTID appears to have two functional lobes, STIM1(448–490) and STIM1(490–530). Homology modeling (Fig. S1 d) suggests that the STIM1(448–490) lobe wraps around and is in contact with the αC helix of SOAR, whereas the STIM1(490–530) lobe does not contact SOAR but bulges from the STIM1(448–490) lobe. STIM1(448–490) and STIM1(490–530) cooperate to control access of SARAF to SOAR. Thus, deletion of STIM1(448–490) and, in particular, STIM1(447–460) and STIM1(475–490) markedly enhances interaction of SARAF with STIM1 (Fig. 3 e), suggesting that deletion of STIM1(448–490) results in STIM1 conformation in which SARAF can access SOAR to inhibit Orai1 and Ca²⁺ influx. Hence, the STIM1(448–490) lobe functions to restrict access of SARAF to SOAR. In contrast, deletion of the STIM1(490–530) prevents access of SARAF to SOAR (Figs. 3 and 5), suggesting that the STIM1(490–530) lobe directs SARAF to SOAR. The four glutamates of CC1 appear to be in contact with the STIM1(448–490) lobe and their mutation likely disrupts the wrapping of SOAR αC helix by the STIM1(448–490) to restrict access of SARAF to SOAR, resulting in an active STIM1.

An interesting finding is that SOAR alone binds SARAF, yet all activated forms of STIM1 that expose SOAR prevent access of SARAF to SOAR. This suggests a potential dynamic regulation of STIM1 function by SARAF. It is clear that SOAR is occluded in STIM1 or the ERM domain by CC1 (Muik et al., 2011) that is likely mediated by the inhibitory helix containing the four glutamates (Yang et al., 2012). CTID may stabilize this conformation and direct SARAF to SOAR to set the STIM1 inactive state. Once SOAR is released by unfolding of the structure, SARAF access to SOAR is restricted, at least transiently, to set the STIM1 active state. SARAF should regain access to
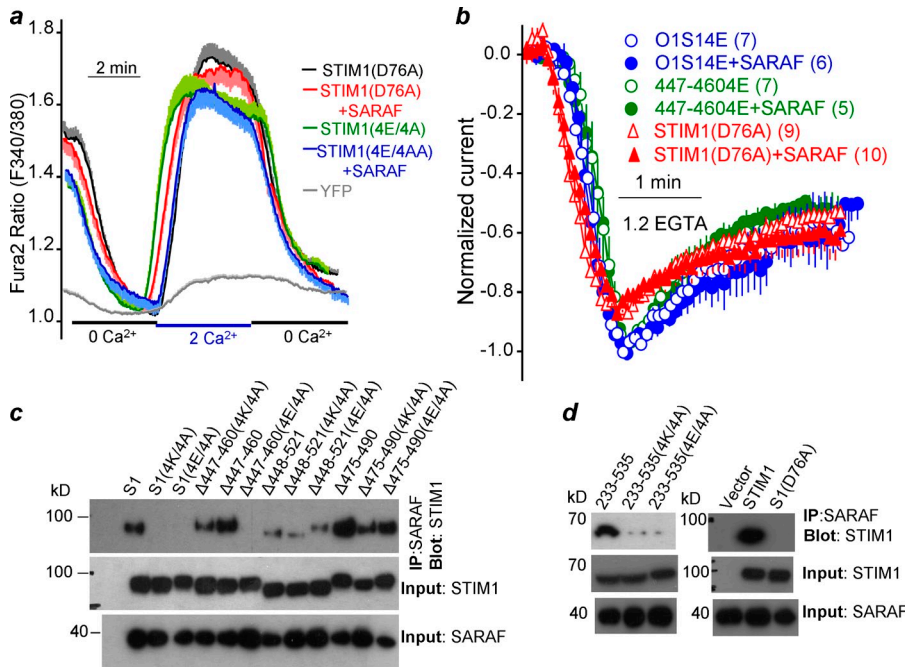
Figure 6. **Orai1 current activated by constitutively active STIM1 mutants shows minimal SCDI and is not affected by SARAF.** HEK cells were transfected with Orai1 and STIM1(4E/4A) or STIM1(D76A) and with or without SARAF. The mean traces of store-independent Ca^{2+} influx (a) and the Orai1 current (b). The results in a and b are given as mean ± SEM of 30–40 cells (a) or the number of cells indicated in parentheses (b). SCDI of Orai1 activated by STIM1 (4E/4A) and STIM1(D76A) is minimal and SARAF does not inhibit the Orai1-dependent Ca^{2+} influx and does not affect the SCDI. (c and d) Coimmunoprecipitation of STIM1, the STIM1 deletion mutants Δ447–460, Δ475–490, and Δ448–521, STIM1(233–535), and their 4K/4A and 4E/4A mutants with SARAF. Note that both the 4K/4A and 4E/4A mutants markedly reduce interaction of SARAF with STIM1 and constructs.

SOAR to be able to facilitate the SCDI. Because SOAR can fully activate Orai1 (Yuan et al., 2009), the conformation of SOAR domain alone must be the active conformation. Because SOAR alone binds SARAF (Fig. 3), it is possible that it represents the active SOAR conformation in STIM1 that regains access to SARAF. This interpretation has some support in the observation that SARAF interaction with STIM1 is enhanced by store depletion (Palty et al., 2012).

Based on the present findings we suggest that in the resting, inactive state when the stores are filled with Ca^{2+} the CC1-SOAR-CTID domains of STIM1 are in a conformation in which the CTID lobes allow access of SARAF to SOAR to keep SOAR in an inactive state. Activation of STIM1 by store depletion or by the mutants STIM1(ΔCTID), STIM1(D76A), and STIM1(4E/4A) releases SARAF to activate STIM1 and Ca^{2+} influx. An additional conformational transition of STIM1 that is likely facilitated by the STIM1(490–530) lobe may result in partial reinteraction of SARAF with SOAR to mediate the SCDI. In this model SARAF not only mediates the SCDI but also serves to keep STIM1 in an inactive state when the stores are filled with Ca^{2+}. Further studies are needed to test this hypothetical model.

Materials and methods

Solutions, reagents, and clones
The STIM1, Orai1, and SOAR clones have been previously described (Yuan et al., 2009). STIM1 clone was generated by cloning into pCDNA7.1GFP at EcoRI (5′) and NotI sites (3′) sites. SOAR was generated by PCR and cloned into pEGFP-C1 (Takara Bio Inc.) vector using EcoRI (5′ and 3′) site. Orai1 clone was generated by cloning into Red-p3xFLAG vector at the NotI (5′) and SalI (3′) sites. The mcherry-Red is downstream and next to the 3× Flag and was cloned into the HindIII site. The STIM1 C-terminal fragment 445–550 was PCR cloned into pEGFP-C1 (Takara Bio Inc.) vector at BglII (5′) and HindIII (3′)sites with EGFP tag at the N terminus. The STIM1 deletion mutants were generated using the QuikChange XL II site-directed mutagenesis kit. The primers were obtained from Integrated DNA Technologies. All point mutations were generated using the

QuikChange Lightning site-directed mutagenesis kit from Agilent Technologies. The human TMEM66 clone (SARAF) was obtained from Thermo Fisher Scientific (GenBank accession no. BC015012.1). TMEM66 was PCR cloned into pCMV6-AC-myc plasmid (OriGene) at HindIII (5′) and MluI (3′) sites with Myc tag at the C terminus. The polyclonal anti-GFP and HRP-conjugated anti-GFP primary antibodies and the HRP-conjugated secondary antibodies were obtained from Life Technologies. The monoclonal anti-Myc antibody was obtained from Cell Signaling Technology.

siRNA and RT-PCR
The scrambled RNA sequence used as control for siRNA experiments was 5′-CGUAAUCGCGUAAUACGCGUAT-3′ (sense) and 5′-AUACGCGU-AUUArCrGCGAUUAACGAC-3′ (antisense) and the siRNA duplex for TMEM66 was 5′-CCAGGAGACGAUAAAGUAGAAAGTT-3′ (sense) and 5′-AACUUUCUACUUUUAUCGUCUCCUGGUA-3′ (antisense). HEK293 cells were plated at 70–80% confluence and transfected with duplexes after 12 h (100 nM/well) in a 6-well plate. The cells were harvested after 48 h; RNA was extracted using the TRIZOL reagent and the mRNA levels were determined by quantitative PCR as described in Seth et al. (2009). In brief, isolated mRNA was reverse-transcribed into cDNA by the iscript cDNA synthesis kit from Bio-Rad Laboratories. The cDNA from the control and siRNA transfected cells was used for quantitative RT-PCR. The primers for quantitative RT-PCR for TMEM66 and GAPDH were purchased from Applied Biosystems. The fold change in the transcript levels of TMEM66 was calculated by normalizing the Ct values from control and siRNA-transfected cells (threshold values) to GAPDH. The plasmids for the STIM1 and mutants were transfected after 48 h of siRNA transfection and the cells were imaged for Ca^{2+} or used for current measurement after 12 h of transfection.

Western blotting and coimmunoprecipitation
Coimmunoprecipitation and Western blotting were performed as described in Yuan et al. (2009). In brief, the cells were harvested in 500 µl of binding buffer (PBS containing 1 mM $NaVO_3$, 10 mM NaPyrophosphate, 50 mM NaF, pH 7.4, and 1% Triton X-100), sonicated, and spun down at 30,000 g for 20 min. For the coimmunoprecipitation experiments, Myc antibody (1 µg) was added to 100 µl of cell extract and incubated overnight at 4°C. 50 µl of 1:1 slurry of protein G Sepharose 4B beads was added to the antibody–extract mix and incubated for an additional 4 h at 4°C. Beads were washed three times for 10 min with binding buffer and proteins were released from the beads with 50 µl of SDS loading buffer. Protein was loaded onto 8% tris-glycine SDS-PAGE gels, which was transferred onto polyvinylidene fluoride membrane for Western blot analysis.

Measurement of Ca^{2+} concentration
The concentration of intracellular Ca^{2+} was measured ~12 h after transfection using a TILL photonics Ca^{2+} imaging system. Intracellular Ca^{2+} was

measured by loading the cells with Fura2. Fura2 fluorescence was recorded at excitation wavelengths of 340 and 380 nm and collecting the light emitted at wavelength above 500 nm. Cells were plated on coverslips that form the bottom of a perfusion chamber and were continuously perfused with a worm (37°C) solution. The standard bath solution contained 140 mM NaCl, 10 mM Hepes, 10 mM glucose, 5 mM KCl, 1 mM MgCl$_2$, and either 1 mM CaCl$_2$ or 0.2 mM EGTA (Ca^{2+}-free). When desired, Ca^{2+} store depletion was achieved by treating the cells with 25 µM cyclopiasonic acid, a SERCA pump inhibitor. Changes in Ca^{2+} are given as the changes in Fura2 340/380 ratios. Results are presented as the mean ± SEM of results from at least three experiments and 30–60 cells.

Confocal imaging

HEK293 cells were plated on glass bottom plates (MatTek Corporation) and transfected with tagged STIM1-YFP, STIM1-CFP, or the mutants and SARAF-YFP for 12–16 h. The images were captured at room temperature with a confocal system (FV1000; Olympus) equipped with a UplanSApo 60× oil immersion objective (NA 1.35; Olympus) at 4× zoom. Images were processed with Photoshop CS3 (Adobe).

Electrophysiology

HEK293T cells were maintained in Dulbecco's modified Eagle's medium and 10% fetal bovine serum. Cells were transiently transfected using Lipofectamine 2000 (Invitriogen) with Orai1, STIM1, or the STIM1 mutants with or without SARAF in a 1:2:2 ratio for 12–24 h at 37°C. To reduce Ca^{2+} toxicity in all constitutively active mutants, the cells were maintained in media supplemented with 1.5 mM EGTA to reduce the free Ca^{2+} concentration.

On the day of experiment, transfected cells were plated on square coverslips in 35-mm Petri dishes and incubated with culture media for at least 1 h to allow attachment to the coverslip. Experiments were performed at room temperature using the tight-seal whole-cell configuration. Patch clamp pipettes were pulled from glass capillaries (Warner Instruments) using a vertical puller (PC-10; Narishige) and had a resistance of 5–7 MΩ when filled with the pipette solution. Whole cell currents were recorded using an Axopatch 200B amplifier (Molecular Devices) with low-pass filtering at 1 kHz. The currents were digitized at a sampling frequency of 5 kHz and stored directly to a hard drive by Digidata 1322 (Axon Instruments). The capacitance transient current was compensated for by using the Axopatch 200B amplifier. Current recording was done with PClamp 10 software, and analysis was done with the help of Clampfit software. The current was recorded by 400-ms rapid alterations of membrane potential from −100 to +100 mV from a holding potential of 0 mV. Subsequent rapid alterations of membrane potentials were spaced at 4-s intervals. FCDI was performed by 1-s voltage steps of −100 mV from a holding potential of 0 mV. Step voltage pulses were applied when current was fully developed. For determination of τ peak currents were taken from the current recorded 3 ms after the start of the pulse to minimize contributions from capacitive current. Steady-state currents were measured at the end of the pulse. The current traces evoked by the −100mV pulse were fitted to a double exponential function to analyze the kinetic parameters as follows: $y = y_0 + A_1 e^{-t/\tau 1} + A_2 e^{-t/\tau 2}$, where y_0 is the steady-state current, A1 and A2 are the relative amplitude of the fast and slow exponentials, respectively, and τ1 and τ2 are the time constants of the corresponding exponentials. The means of multiple experiments are given as mean ± SEM of the number of experiments performed. Differences between groups were analyzed by unpaired Student's t test and significance is considered at p-values <0.05. The current recorded at −100 mV was used to calculate current density as pA/picofarads.

To measure SCDI the pipette solution contained 135 mM CsCl, 6 mM MgCl$_2$, 2 mM MgATP, 1.2 mm EGTA, and 10 mm Hepes, pH 7.2 (with CsOH). For FCDI, 1.2 mM EGTA in the pipette solution was replaced by 10 mM EGTA. To record constitutive current, 1.2 mM EGTA was replaced with 10 mM BAPTA and cells were kept in bath solution containing 1 mM CaCl$_2$. Once whole cell is achieved external solution was rapidly changed to bath solution containing 10 mM CaCl$_2$. In SCDI recording, after establishing the whole cell configuration, the cells were kept in Ca^{2+}-free solution for 5 min to allow store depletion before exposing the cells to bath solution containing 10 mM Ca^{2+}. The standard bath solution contained 130 mM NaCl, 5 mM KCl, 1 MgCl$_2$, and 10 mM Hepes with or without 10 mM CaCl$_2$ (pH 7.4 with NaOH).

Homology modeling

The human C-terminal STIM1 sequence (amino acids 234–685; NCBI Protein database accession no. NM_003156.3) was submitted to the full-chain protein structure prediction server Robetta (Kim et al., 2004) and I-Tasser.

Robetta generated five models and I-Tasser four models. The quality estimates were determined by the Q-mean server (Benkert et al., 2011). This server provides a quality score by two methods. First, it compares the model with statistical properties of known structures. Second, it uses the information contained in ensemble of models for a given sequence using an all against all structural comparison of the model, also called composite scoring. We used the second method for our quality estimation. Q-mean is a parameter between 0 and 1. Scores equivalent to 1 are similar to crystallographic structure. The I-Tasser models had Q-mean scores between 0.2 and 0.25 and were not considered further. The Robetta models had Q-mean scores of 0.449, 0.480, 0.447, 0.431, and 0.430. Although all scores are low, the model with Q-mean score of 0.447 had a confidence of 0.8 and predicted reasonably well the structure of SOAR and the position of the inhibitory helix (see Fig. S1), and was thus considered further. The software completed the model using a de novo modeling source. The coordinates provided by the Robetta server were used to generate the final model with PyMol software (Schrödinger, LLC). Next we aligned the structure of STIM1(344–442) with the recently available crystal structure of SOAR (Yang et al., 2012) in Pymol software (Fig. S1 c). These two structures showed a high degree of alignment.

Online supplemental material

Online supplemental material contains five figures and one table. Figs. S1–S5 show the STIM1 homology model, sequence alignment of CTID, localization of several STIM1 deletion mutants, properties of STIM1(Δ475–490), and elimination of the SARAF-independent SCDI by 10 mM BAPTA. Table S1 summarizes the mean kinetic parameters and extent of FCDI and SCDI. Online supplemental material is available at http://www.jcb.org/cgi/content/full/jcb.201301148/DC1.

References

Benkert, P., M. Biasini, and T. Schwede. 2011. Toward the estimation of the absolute quality of individual protein structure models. *Bioinformatics*. 27:343–350. http://dx.doi.org/10.1093/bioinformatics/btq662

Derler, I., M. Fahrner, M. Muik, B. Lackner, R. Schindl, K. Groschner, and C. Romanin. 2009. A Ca2(+)release-activated Ca2(+) (CRAC) modulatory domain (CMD) within STIM1 mediates fast Ca2(+)-dependent inactivation of ORAI1 channels. *J. Biol. Chem.* 284:24933–24938. http://dx.doi.org/10.1074/jbc.C109.024083

Derler, I., R. Schindl, R. Fritsch, and C. Romanin. 2012. Gating and permeation of Orai channels. *Front. Biosci.* 17:1304–1322. http://dx.doi.org/10.2741/3988

Engh, A., A. Somasundaram, and M. Prakriya. 2012. Permeation and gating mechanisms in store-operated CRAC channels. *Front. Biosci.* 17:1613–1626. http://dx.doi.org/10.2741/4007

Feske, S., Y. Gwack, M. Prakriya, S. Srikanth, S.H. Puppel, B. Tanasa, P.G. Hogan, R.S. Lewis, M. Daly, and A. Rao. 2006. A mutation in Orai1 causes immune deficiency by abrogating CRAC channel function. *Nature*. 441:179–185. http://dx.doi.org/10.1038/nature04702

Hoth, M., and R. Penner. 1993. Calcium release-activated calcium current in rat mast cells. *J. Physiol.* 465:359–386.

Huang, G.N., W. Zeng, J.Y. Kim, J.P. Yuan, L. Han, S. Muallem, and P.F. Worley. 2006. STIM1 carboxyl-terminus activates native SOC, I(crac) and TRPC1 channels. *Nat. Cell Biol.* 8:1003–1010. http://dx.doi.org/10.1038/ncb1454

Kawasaki, T., I. Lange, and S. Feske. 2009. A minimal regulatory domain in the C terminus of STIM1 binds to and activates ORAI1 CRAC channels. *Biochem. Biophys. Res. Commun.* 385:49–54. http://dx.doi.org/10.1016/j.bbrc.2009.05.020

Kim, D.E., D. Chivian, and D. Baker. 2004. Protein structure prediction and analysis using the Robetta server. *Nucleic Acids Res.* 32:W526–W531.

Korzeniowski, M.K., I.M. Manjarrés, P. Varnai, and T. Balla. 2010. Activation of STIM1-Orai1 involves an intramolecular switching mechanism. *Sci. Signal.* 3:ra82. http://dx.doi.org/10.1126/scisignal.2001122

Lee, K.P., J.P. Yuan, W. Zeng, I. So, P.F. Worley, and S. Muallem. 2009. Molecular determinants of fast Ca2+-dependent inactivation and gating of

the Orai channels. *Proc. Natl. Acad. Sci. USA*. 106:14687–14692. http://dx.doi.org/10.1073/pnas.0904664106

Lee, K.P., J.P. Yuan, J.H. Hong, I. So, P.F. Worley, and S. Muallem. 2010. An endoplasmic reticulum/plasma membrane junction: STIM1/Orai1/TRPCs. *FEBS Lett.* 584:2022–2027. http://dx.doi.org/10.1016/j.febslet.2009.11.078

Liou, J., M.L. Kim, W.D. Heo, J.T. Jones, J.W. Myers, J.E. Ferrell Jr., and T. Meyer. 2005. STIM is a Ca2+ sensor essential for Ca2+-store-depletion-triggered Ca2+ influx. *Curr. Biol.* 15:1235–1241. http://dx.doi.org/10.1016/j.cub.2005.05.055

Muik, M., M. Fahrner, R. Schindl, P. Stathopulos, I. Frischauf, I. Derler, P. Plenk, B. Lackner, K. Groschner, M. Ikura, and C. Romanin. 2011. STIM1 couples to ORAI1 via an intramolecular transition into an extended conformation. *EMBO J.* 30:1678–1689. http://dx.doi.org/10.1038/emboj.2011.79

Mullins, F.M., C.Y. Park, R.E. Dolmetsch, and R.S. Lewis. 2009. STIM1 and calmodulin interact with Orai1 to induce Ca2+-dependent inactivation of CRAC channels. *Proc. Natl. Acad. Sci. USA*. 106:15495–15500. http://dx.doi.org/10.1073/pnas.0906781106

Palty, R., A. Raveh, I. Kaminsky, R. Meller, and E. Reuveny. 2012. SARAF inactivates the store operated calcium entry machinery to prevent excess calcium refilling. *Cell*. 149:425–438. http://dx.doi.org/10.1016/j.cell.2012.01.055

Parekh, A.B. 1998. Slow feedback inhibition of calcium release-activated calcium current by calcium entry. *J. Biol. Chem.* 273:14925–14932. http://dx.doi.org/10.1074/jbc.273.24.14925

Parekh, A.B., and J.W. Putney Jr. 2005. Store-operated calcium channels. *Physiol. Rev.* 85:757–810. http://dx.doi.org/10.1152/physrev.00057.2003

Park, C.Y., P.J. Hoover, F.M. Mullins, P. Bachhawat, E.D. Covington, S. Raunser, T. Walz, K.C. Garcia, R.E. Dolmetsch, and R.S. Lewis. 2009. STIM1 clusters and activates CRAC channels via direct binding of a cytosolic domain to Orai1. *Cell*. 136:876–890. http://dx.doi.org/10.1016/j.cell.2009.02.014

Roos, J., P.J. DiGregorio, A.V. Yeromin, K. Ohlsen, M. Lioudyno, S. Zhang, O. Safrina, J.A. Kozak, S.L. Wagner, M.D. Cahalan, et al. 2005. STIM1, an essential and conserved component of store-operated Ca^{2+} channel function. *J. Cell Biol.* 169:435–445. http://dx.doi.org/10.1083/jcb.200502019

Seth, M., Z.S. Zhang, L. Mao, V. Graham, J. Burch, J. Stiber, L. Tsiokas, M. Winn, J. Abramowitz, H.A. Rockman, et al. 2009. TRPC1 channels are critical for hypertrophic signaling in the heart. *Circ. Res.* 105:1023–1030. http://dx.doi.org/10.1161/CIRCRESAHA.109.206581

Stathopulos, P.B., L. Zheng, G.Y. Li, M.J. Plevin, and M. Ikura. 2008. Structural and mechanistic insights into STIM1-mediated initiation of store-operated calcium entry. *Cell*. 135:110–122. http://dx.doi.org/10.1016/j.cell.2008.08.006

Stathopulos, P.B., L. Zheng, and M. Ikura. 2009. Stromal interaction molecule (STIM) 1 and STIM2 calcium sensing regions exhibit distinct unfolding and oligomerization kinetics. *J. Biol. Chem.* 284:728–732. http://dx.doi.org/10.1074/jbc.C800178200

Vig, M., C. Peinelt, A. Beck, D.L. Koomoa, D. Rabah, M. Koblan-Huberson, S. Kraft, H. Turner, A. Fleig, R. Penner, and J.P. Kinet. 2006. CRACM1 is a plasma membrane protein essential for store-operated Ca2+ entry. *Science*. 312:1220–1223. http://dx.doi.org/10.1126/science.1127883

Yang, X., H. Jin, X. Cai, S. Li, and Y. Shen. 2012. Structural and mechanistic insights into the activation of Stromal interaction molecule 1 (STIM1). *Proc. Natl. Acad. Sci. USA*. 109:5657–5662. http://dx.doi.org/10.1073/pnas.1118947109

Yuan, J.P., W. Zeng, M.R. Dorwart, Y.J. Choi, P.F. Worley, and S. Muallem. 2009. SOAR and the polybasic STIM1 domains gate and regulate Orai channels. *Nat. Cell Biol.* 11:337–343. http://dx.doi.org/10.1038/ncb1842

Zhang, S.L., A.V. Yeromin, X.H. Zhang, Y. Yu, O. Safrina, A. Penna, J. Roos, K.A. Stauderman, and M.D. Cahalan. 2006. Genome-wide RNAi screen of Ca(2+) influx identifies genes that regulate Ca(2+) release-activated Ca(2+) channel activity. *Proc. Natl. Acad. Sci. USA*. 103:9357–9362. http://dx.doi.org/10.1073/pnas.0603161103

Zweifach, A., and R.S. Lewis. 1995. Slow calcium-dependent inactivation of depletion-activated calcium current. Store-dependent and -independent mechanisms. *J. Biol. Chem.* 270:14445–14451. http://dx.doi.org/10.1074/jbc.270.24.14445